Frontiers in Scientific Research and Technology

Online ISSN: 2682-2970
Print ISSN: 2682-2962
http://fsrt.journals.ekb.eg

FSRT J 9 (2024) 80 - 99 10.21608/FSRT.2024.305628.1133

Assessment of Middle Jurassic sedimentary sequence's petroleum system at Imhotep-W-1X well, Northwestern desert, using integrated geochemical, geomechanics, XRD, and basin modeling

Walaa A. Ali[1]* and Mohamed Fagelnour[2]

[1] Petroleum Geology Department, Faculty of Petroleum and Mining Sciences, Matrouh University, 51511, Matrouh, Egypt

[2] Khalda Petroleum Company, Cairo, Egypt

ARTICLE INFO

Article history:
Received 19 July 2024
Received in revised form 22 July 2024
Accepted 23 July 2024
Available online 30 July 2024

Keywords
XRD,
geomechanics,
burial history model,
TOCΔlogR,
Imhotep Field,
Matruh Basin,
Khatatba Formation,
Western Desert,
Egypt.

ABSTRACT

This study analyzes the petroleum potential of the Middle Jurassic Khatatba Formation (Fm) in the Matruh Basin, northwestern Egypt. Climate changes and Tethyan Ocean sea level oscillations deposited fine and coarse clastics in this formation under semi-arid and semi-humid conditions, demonstrating in situ dual source and reservoir characteristics. Maturation of the source rocks was related to Late Jurassic–Early Cretaceous Tethyan rifting. The onset of oil generation occurred in the Early Cretaceous (~ 125 Ma), while the onset of gas generation happened in the Late Cretaceous (~ 95 Ma). Shales from the Lower Cretaceous Alam El Bueib Formation are the primary sealing rocks, while carbonates and shales from the Khatatba Formation are secondary sealing rocks. Trap types are structural, created during the Late Jurassic and Early Cretaceous rifting of the Matruh Basin. The Upper Safa Member sandstones show an upward trend in kaolinite concentration and demonstrate low-quality, tight sandstone reservoirs. The Lower Safa Member sandstones indicate greater gas reservoir quality with lower shale quantities. Overall, the petroleum system of the Khatatba Formation proves generally fair hydrocarbon potential in the studied well. The objectives of this study are to assess the hydrocarbon potential of the Khatatba Formation in the Imhotep-W-1X well, Matruh Basin, utilizing multi-integration analysis of X-ray diffraction, XRD, basin modeling, geomechanics, and geochemical analysis.

1. Introduction

The Matruh Basin contains approximately 23 billion barrels of oil equivalent (BBOE) of proven oil and about 3 TCF of gas reserves (Metwalli et al., 2018). The Mesozoic source rocks in the Matruh Basin are the Middle Jurassic Khatatba, the Lower Cretaceous Alam El Bueib, and the Upper Cretaceous "G" Member of the Abu Roash formations (Gentzis et al., 2018; Fello et al., 2024; Ali et al., 2024). The primary Mesozoic hydrocarbon reservoir rocks in the Matruh Basin include the Khatatba and Alam El Bueib sandstones, the Aptian Alamein Dolomites, the Albian Kharita and lower Cenomanian Bahariya sandstones, and the Abu Roash formations' "G" Member (Metwalli and Pigott, 2005 ; Fello et al., 2024). Several possibilities in the Matruh Basin (El-Shorbagy et al., 2023) have indicated the presence of the petroleum system. One of these is the Imhotep potential, which lies on a series of N-NE trending ridges and faults and is the key structural trend of the finds in this area. The Middle Jurassic Khatatba Formation was modeled by Ali and Fagelnour (2023) for its hydrocarbon source rock potential in the Matruh Basin utilizing geological and geochemical data from the Apidose-1X well.

* Corresponding author at Matrouh University

E-mail addresses: walaa.ali@mau.edu.eg (Walaa A. Ali)

Formation works as an effective oil and gas source rock, with oil generation starting in the Early Cretaceous and gas generation beginning in the Late Cretaceous. The Matruh Basin comprises all features of a petroleum system, in which creation, movement, and accumulation began in the Early Cretaceous, with hydrocarbons filling traps during the rifting periods. Moreover, Ali (2023) examined the depositional environment and paleoclimate of the Khatatba Formation in Matruh Field using organic and inorganic data from two wells (Matruh-5 and Matruh-6). Using elemental data, Ali (2023) analyzed the provenance and sedimentation circumstances responsible for the accumulation of Middle Jurassic source rocks. The interpretation indicated that the Khatatba Formation source rocks were generated during a marine regression and recognized the Upper and Lower Safa members as the most significant source rocks in the Matruh Field. Based on the aforementioned investigations, it is obvious that the Khatatba Formation contains numerous key source and reservoir rocks of various grade and thickness over different regions of the Matruh Basin. This indicates the necessity to conduct out more extensive and integrated investigations in diverse hydrocarbon potential regions prior to beginning exploration and production activities in unstudied and/or underexplored concession areas.

The objective of this study is to evaluate the hydrocarbon potential of the Khatatba Formation in the Imhotep-W-1X well, located in the Matruh Basin. This will be achieved through the use of a comprehensive analysis that combines X-ray diffraction (XRD), basin modeling, geomechanics, and geochemical analysis.

2. Geological setting and lithostratigraphy

The geological history and setting of the northwestern Desert of Egypt reflect, in part, the tectonostratigraphic evolution of the unstable shelf, which represents the northeastern part of the African Craton (Fig. 1). The Western Desert's hydrocarbon occurrence is closely related to past tectonic and stratigraphic events, which formed a combination of source, reservoir, and seal rocks. According to (Metwalli et al., 2018), the northern part of Egypt experienced three different tectonic events. The first event created a NW or WNW fault trend during the Paleozoic–Early Mesozoic (Triassic). The second event occurred during the Late Mesozoic (Cretaceous) and formed the E-NE Syrian Arc System, which consists of a series of faulted anticlines of different dips and directions. Finally, the third tectonic event developed throughout the Early Cenozoic (Late Eocene and Early Oligocene) and created the NW Gulf of Suez and NNE Aqaba fault trends. Various geological studies dealt with the tectonic framework, stratigraphy, facies distribution, and development of sedimentary basins in the North Western Desert (Guiraud and Bosworth, 1999; Shalaby et al., 2014; Bosworth and Tari, 2021; Ali et al., 2024). The deposition of the sedimentary succession in the Matruh Basin was governed by the regional tectonics related to the drift of the African plate and rifting of the Tethyan Ocean. This caused the accumulation of thick sedimentary successions, which are separated into four main depositional sequences "DSQ" (Fig. 2). The Khatatba Formation in the Imhotep W-1X well is characterized, from the base to the top, by clastics of the Lower Safa and Upper Safa members, which are separated by thick carbonates of the Kabrit Member. The carbonates of the Zahra Member represent the uppermost part of the Khatatba Formation.

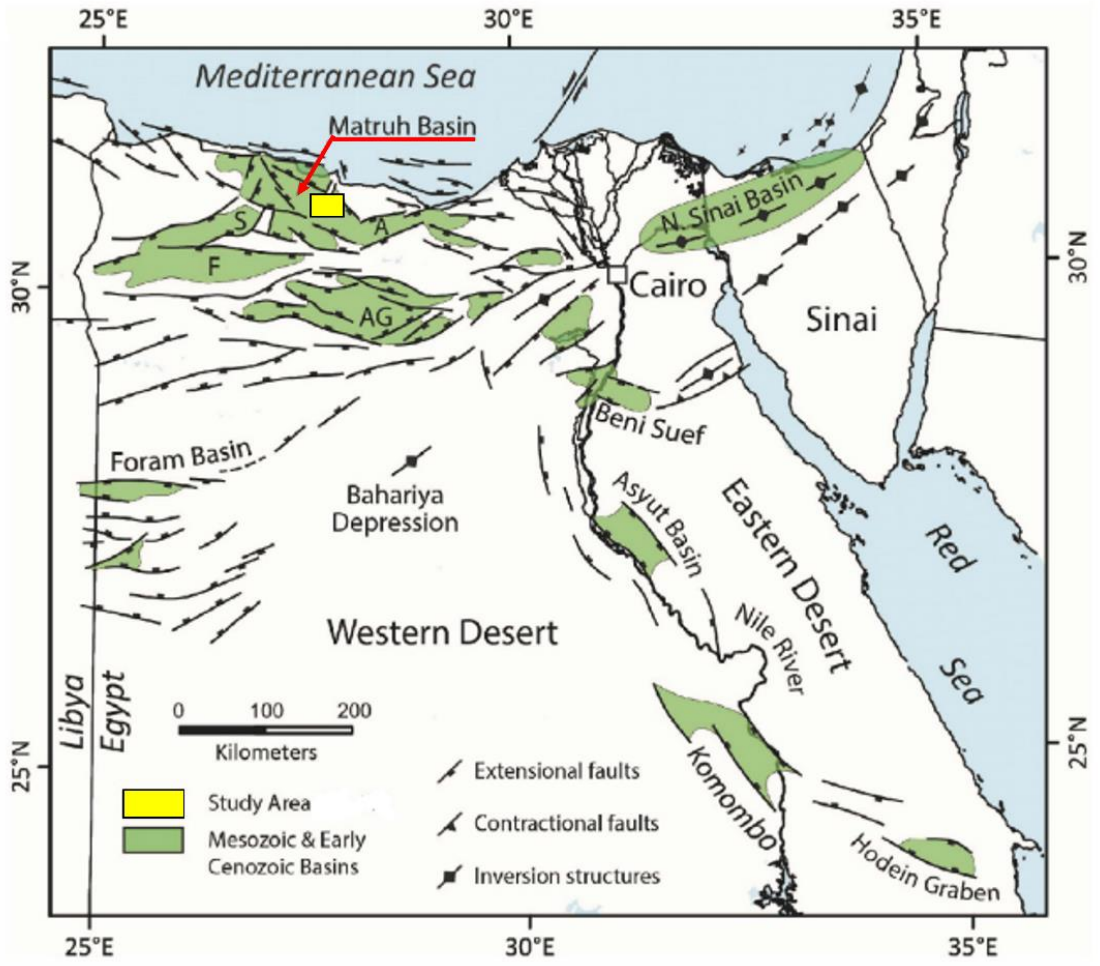

Fig. 1. Location map of the Matruh Basin along with other Mesozoic and Early Cenozoic basins in the North Western Desert of Egypt (after, Bosworth et al. 2015 & Yousef et al., 2023).

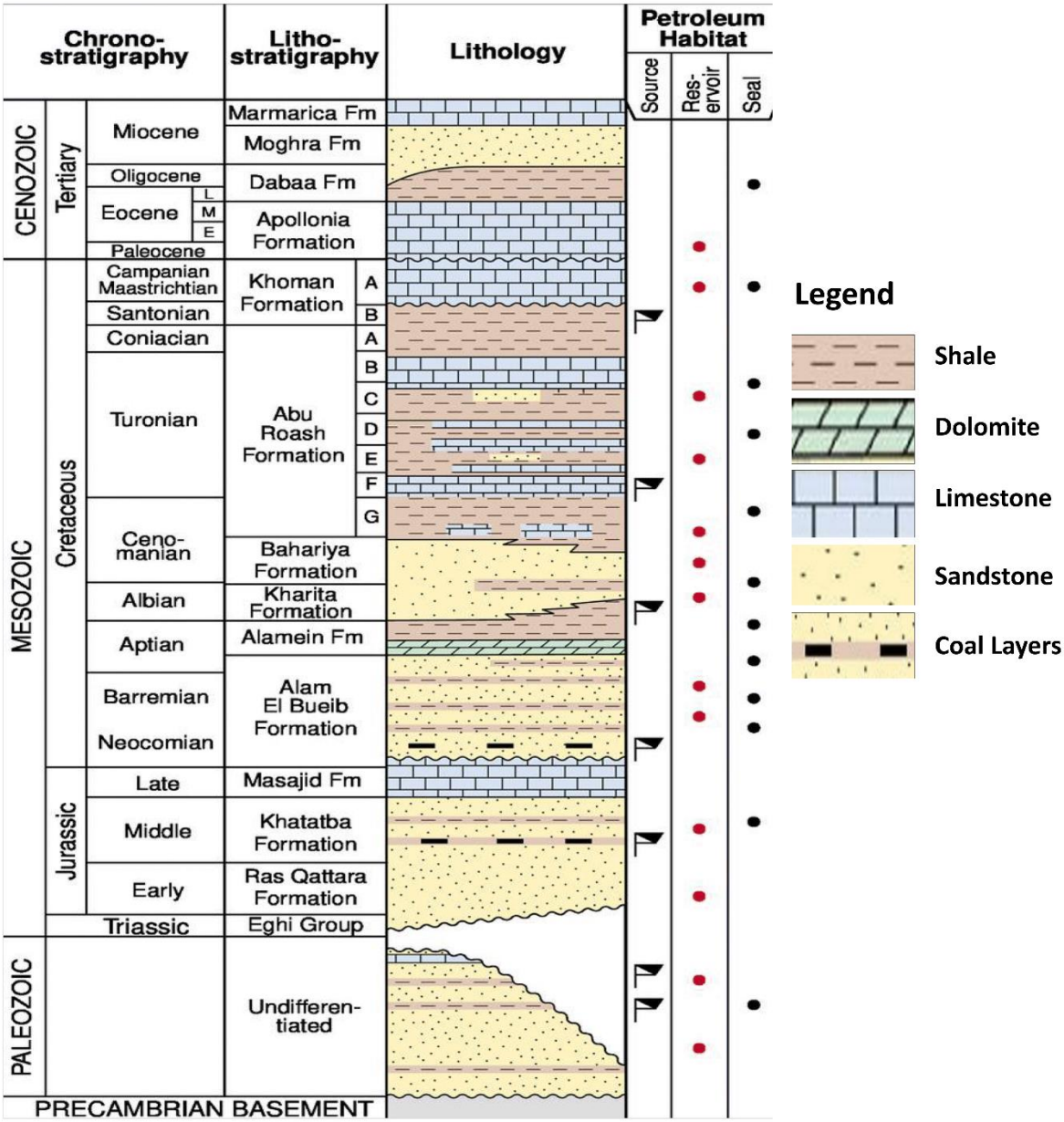

Fig. 2. Stratigraphic column of the North Western Desert, Egypt, showing the main lithostratigraphy units, lithology, age, and formation's petroleum system elements (modified After EGPC, 1992, & Schlumberger 1995).

3. Methodology and analyses

This section describes the sampling, clay fraction mineralogy, and organic petrography/vitrinite reflectance, total organic carbon calculated from well logs, geomechanics workflow, and basin modelling.

3.1 Samples

A total number of 14 samples from the Imhotep W-1X well were provided by the Egyptian General Petroleum Corporation (EGPC) for the current study. The source rock samples were selected from fine-grained lithologies that provided high gamma-ray (GR) responses on the electrical logs, while the reservoir samples were selected from coarse-grained lithologies that provided low GR log responses. To interpret the main lithology of the selected samples, a correction of the depth shift between the electrical and mud logs was conducted. The samples from the Imhotep W-1X well were selected at different levels of the Khatatba Formation in such a way as to be representative of different lithologies (shale, sandstone, carbonates), which reflect changes in the depositional environment. Palynologically productive samples (not pure sandstones/carbonates) were also selected to complement the organic geochemical analysis with organic petrographic analysis for a better interpretation of the source rock potential.

3.2. Clay fraction X-Ray diffraction (XRD) analysis

The clay fractions extracted from three specific samples (#1 at depth 4769.6 m, #9 at depth 4522.7 m, and #11 at depth 4480.0 m) representing the Lower and Upper Safa members were analyzed using X-ray diffraction (XRD) to accurately determine the mineral composition. The analysis was conducted at the Central Metallurgical Research Institute (CMRDI) Central Laboratory Sector using an automated powder diffractometer system of Philips type Pan Alytica X-pert-pro. The interpretation was conducted with APD and PDF software, which incorporate powder diffraction and PDf-2 Database Sets 1–45 following (Khalda, 2014, Bunaciu et al., 2015, Hassan and Baioumy, 2006).

3.3. Vitrinite reflectance under reflected white light (RWL)

Vitrinite reflectance measurements were made on Sample 7 (Depth: 4614.1m) at the Advanced Technology Center, Core Laboratories, Houston, TX, United States. Fifty vitrinite reflectance measurements (VRo % (were randomly collected on primary vitrinite using a ×50 oil immersion objective with a refractive index (noil) of 1.514 at a temperature of 23 °C and a glass standard having Ro of 1.359%. Representative particles were photomicrographed using a digital camera (Fig.3). The categorization of palynomacerals into vitrinite and liptinite macerals using RWL microscopy was conducted according to the ICCP System (Sýkorová et al., 2005; Pickel et al., 2017.

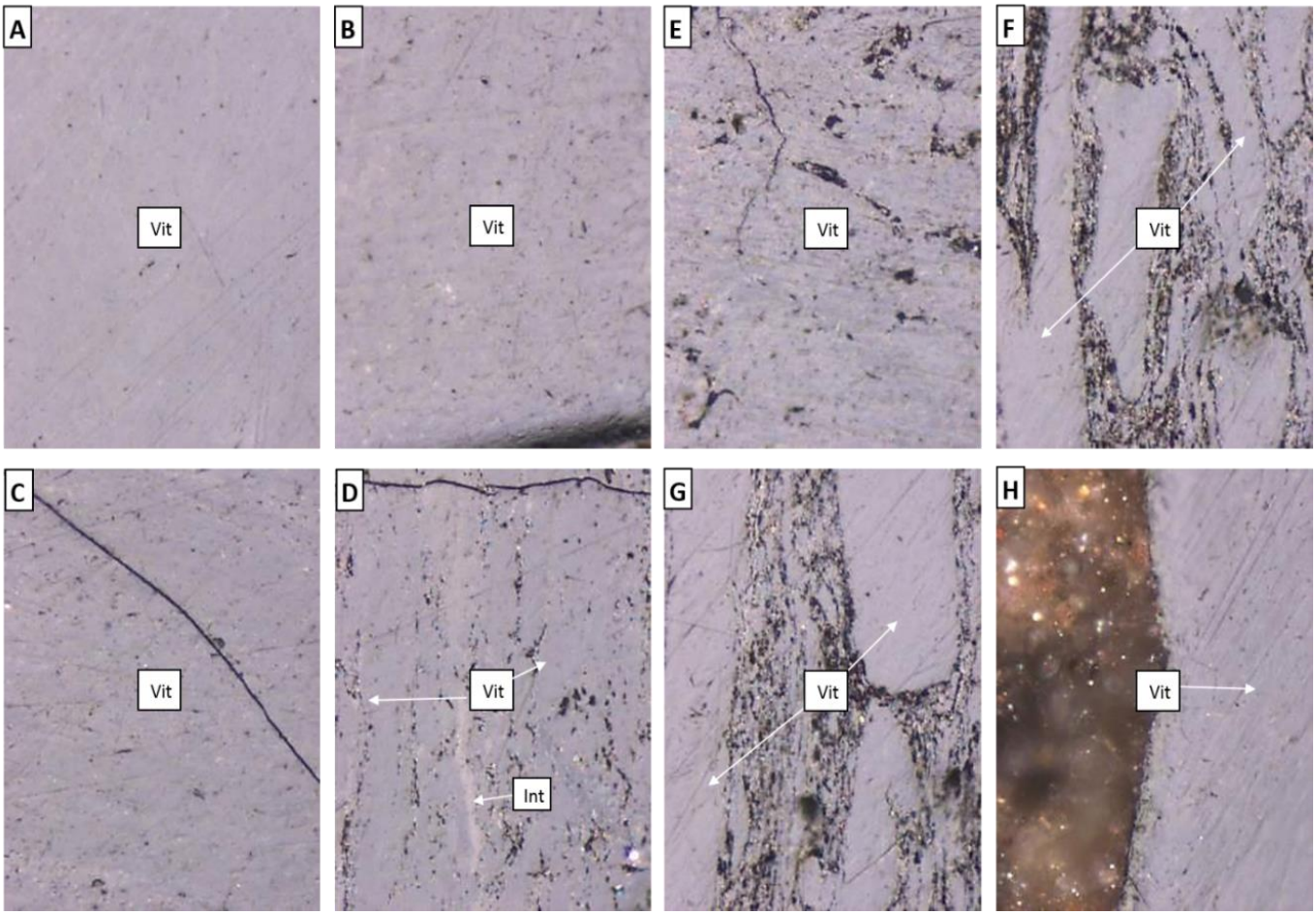

Fig. 3. Photomicrographs of organic matter recovered from the Khatatba Formation deposits in the Imhotep W-1X well. Sample 7 (depth 15143.5 m) was taken under reflected white light (RWL). (A): Primary vitrinite (Vit) in the form of collotelinite has a Ro of 1.37%. (B): Vitrinite (Vit) as collotelinite with a VRo value of 1.33%. (C): As with (A) and (B), the VRo value is 1.35%. (D): Vitrinite with a VRo value of 1.37% enclosing inertinite (Int). (E): vitrinite as collotelinite with a VRo value of 1.32%. (F): Vitrinite with a VRo of 1.39% is associated with clay minerals. (G): Same as (F). (H): Vitrinite band (collotelinite) having a VRo value of 1.38%.

3.4. TOC ΔlogR calculations from well log

The method used to calculate the total organic carbon (TOC) was explained by (Passey et al., 1990) as the resistivity-porosity overlay approach. The displayed curves are arranged in a manner that results in their alignment in the non-source area. The interval between these curves is often known as the ΔlogR and is utilized for the identification of intervals rich in organic matter (Fig. 4). The calculation of organic richness may be performed by employing a combination of resistivity and one of the porosity logs, such as sonic, density, or neutron. In the present investigation, the baseline value for Δt was determined to be 77.826 μs/m, whereas the baseline value for resistivity was established as 5.7148 ohm-m. The method of overlaying curves may also be used for neutron and density logs as explained by (Passey et al., 1990).Nevertheless, the utilization of sonic technology is recommended due to its superior capability for in-depth investigation and its reduced susceptibility to the influence of well conditions. Moreover, utilizing the sonic log in conjunction with density and/or resistivity logs or calibrating it with core data, can enhance the accuracy and reliability of the results ((Meyer and Nederlof, 1984).The total organic carbon (TOC) for Imhotep-W-1X well within the depth range of 4305-4786 m was calculated using (**Eq.1**). In case a sonic log is not available, density and neutron logs can be utilized, only if the borehole is in good condition with no washout to overlay with the resistivity log, as illustrated in the equations (Eqs. 2, and 3).

$$\Delta\log R_{Sonic} = \log_{10}(R/R_{Baseline}) + 0.02\times(\Delta t - \Delta t_{Baseline}) \quad \textbf{(Eq.1)}$$

$$\Delta\log R_{Neu} = \log_{10}(R/R_{Baseline}) + 4\times(\Phi_N - \Phi_{N\ Baseline}) \quad \textbf{(Eq.2)}$$

$$\Delta\log R_{Den} = \log_{10}(R/R_{Baseline}) + 2.5\times(\rho_b - \rho_{\ Baseline}) \quad \textbf{(Eq.3)}$$

The value of constant C was modified to TOC=Δ log R×10 (2.297-0.15*9). The three porosity logs, sonic, neutron, density, were tested but in the current study, the resistivity-sonic overlay was used for the computation of TOC as illustrated in (Eq. 4) as follows:

$$TOC = \Delta\log R \times 10^{(2.297-0.1688\times LOM)} \quad \textbf{(Eq. 4)}$$

Where; LOM is the level of maturity, the Δ log R is function of maturity and TOC as shown in (Eq. 5) and the constants 2.297 and 0.1688 are parameters determined empirically in clay rich rock by (Passey et al., 1990)**.**

$$\Delta\log R = \log_{10}(R/R_{Baseline}) + C \times (\Delta t - \Delta t_{Baseline}) \quad \textbf{(Eq. 5)}$$

Where: Δ log R is the separation measured in the logarithmic resistivity cycle, R is the resistivity measured in ohm-m by the logging tool, Rbaseline is the resistivity corresponding to the Δtbaseline values when the curves are base-lined in non-source, clay-rich rocks, as in the Zahra Member (Fig. 4A) and the Lower Safa Member (Fig. 4B), and C is the constant (ratio between scales of the resistivity and sonic log) = 0.02. LOM is the level of maturity calculated from %VRo data using the Henderson petrophysics conversion graph, and is 11.2 as illustrated in (Fig. 4C).

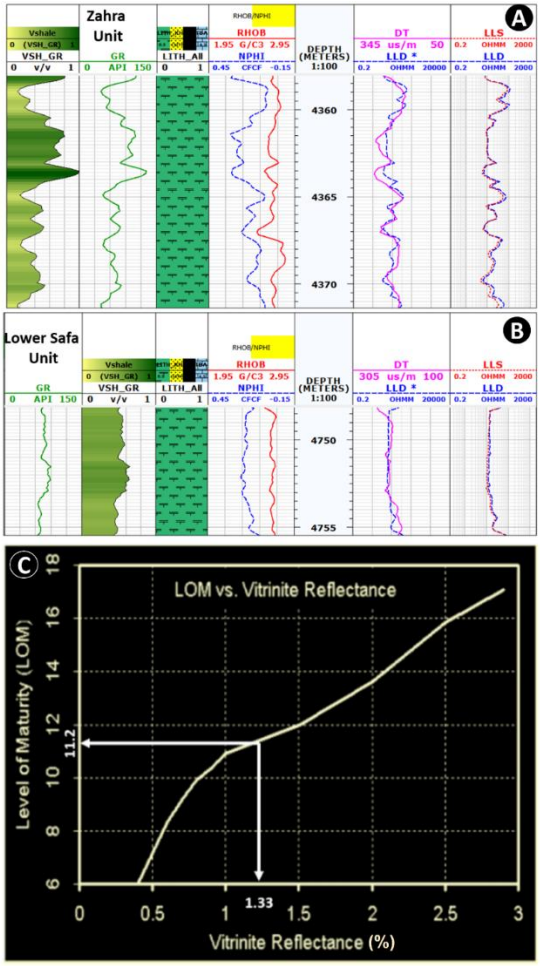

Fig. 4. The resistivity-sonic curves overlay technique (Track 6) was used to figure out how rich in organic matter the well logs were in two different units of the Khatatba Formation, **(A):** Zahra Member and **(B):** the Lower Safa Member along the Imhotep W-1X well. **(C):** Henderson petrophysics conversion graph for converting VRo % into LOM. LOM corresponding to a (measured) maturity value of 1.33% VRo is estimated to be 11.2 (Adapted from: Crain and Holgate, 2014).

3.5. Rock geomechanics

Obtaining rock mechanical parameters allows to characterize the quality and strength of rocks. The estimation of mechanical rock parameters, such as Poisson's ratio (PR) and Young's modulus (YM), is often derived from well logs, which are subsequently calibrated with core data if such data is available. Shale brittleness is among the outcomes derived from geomechanical studies. Shale intervals characterized by elevated brittleness levels are optimal locations for identifying hydraulic fracture initiation. The incorporation of the geomechanical model has the potential to enhance the efficacy of brittleness and

facilitate the optimization of various parameters, such as the selection of perforation intervals, fracture pressure, and geometry.

The datasets used include density, porosity, and compressional and shear slowness (DTC, DTS), which are derived from dipole sonic logs and are considered as important parameters used for determining the Young's modulus and Poisson's ratio. If the DTS log is not available, it is possible to generate a synthetic log by utilizing the equations outlined in (Fig. 5).

Following the procedure described by (Jaeger et al., 2009; Perez and Marfurt, 2014; Schön, 2015; Wu and Grana, 2017; Knippel et al., 2013; Ali, 2024), the workflow established in Figure 5 illustrates the equations used to estimate the rock mechanical properties from well logs. The vertical P-wave velocity (Vp) and vertical S-wave velocity (Vs) were determined by calculating the compressional wave velocity (DTC) and shear wave velocity (DTS), respectively. The Vp/Vs ratio was computed and denoted as VPVS. The calculation of Poisson's ratio was performed using the equation described in Fig. 4 and the computation of shear and bulk moduli was also performed. The calculation of Young's modulus involved the utilization of two equations as illustrated in Figure 4.

According to (Rickman et al., 2008) the concept of brittleness may be understood as a function of two key rock properties: Poisson's ratio (PR) and Young's modulus (YM). The measure of rock brittleness takes into account both PR and YM and provides an indication of the rock's susceptibility to fail. The formation's brittleness increases as the YM value increases and the PR value decreases. As a result, the formation experiences increased fracturing and reduced stress, with a corresponding increase in brittleness. In contrast, the ductile shale intervals exhibit more plasticity and need elevated pressure levels for fracturing to occur. When a rock's ductile behavior is more pronounced than its elastic behavior, it is ductile because it can absorb a significant amount of energy before rupturing. On the other hand, (Perez and Marfurt, 2014) noted that rocks with brittle characteristics exhibit a wider range of elastic behavior and a narrower range of ductile behavior. Shale reservoirs sometimes contain a moderate quantity of organic matter, tiny holes and cracks, and high capillary pressure. Shale acts as a source, a reservoir, and a seal in a shale gas system (Zhu et al., 2019). Shale gas reservoirs may be deemed suitable for commercial exploitation when they possess a brittleness index, namely a quartz content of over 40%, since this facilitates more effective fracturing (Delle Piane et al., 2018; Zou et al., 2021) proposed that gas can adhere to both organic matter and mineral grains within shale formations. This keeps the gas inside the pores, cracks, fissures, and joints of the shale. Thus, successful production of gas from shale reservoirs depends mainly on successful penetration of the structured network of fractures.

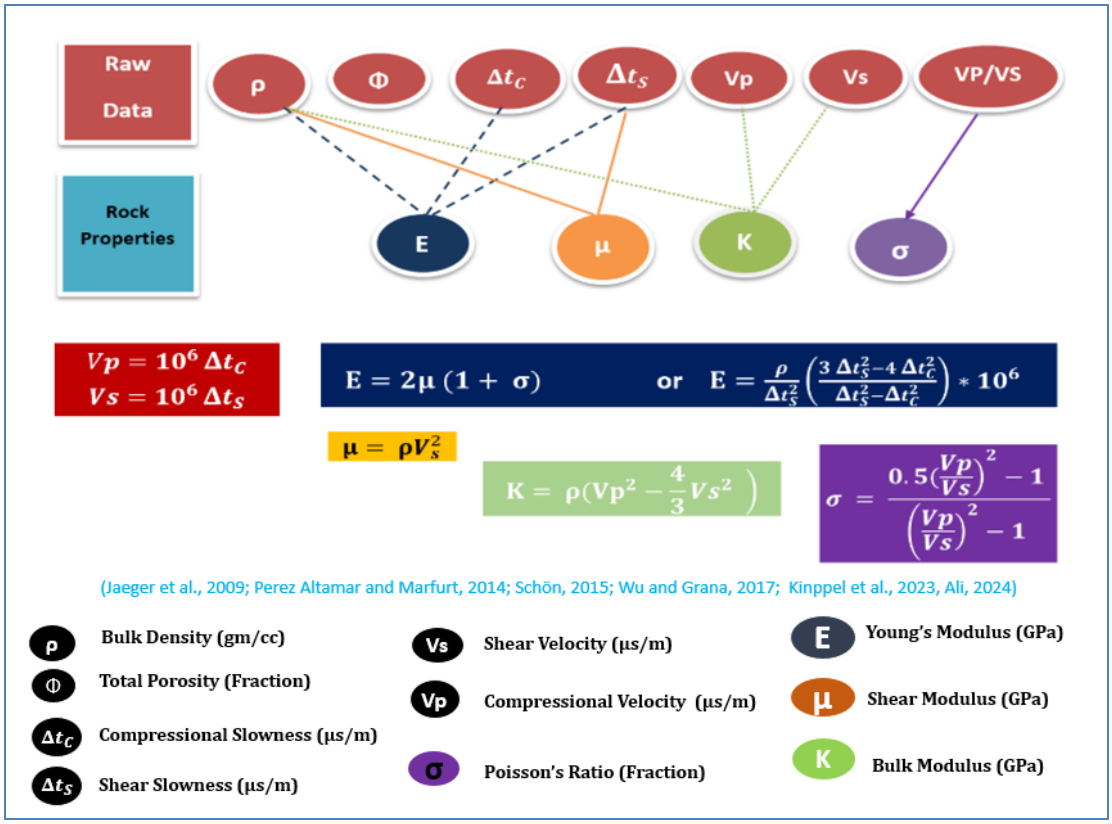

Fig. 5. The workflow of the rock mechanics assessment and used equations to detect the brittle and ductile intervals in the Khatatba Formation at the location of the studied well at Matruh Basin.

3.6. Basin modelling

The dataset comprises composite logs and electric well logs obtained from the Imhotep W-1X well. The composite logs were utilized to obtain information on the depths, thicknesses, and nomenclature of the formations under investigation, which were then used in the development of 1-D burial history model (Waples, 1985). The electric well logs were used to obtain the bottom hole temperature (BHT) of 143.8 ^{O}C , and the corrected BHT equals 153.8 ^{O}C after a circulation time reached 12 hours, which was subsequently employed in the computation of the geothermal gradient (28.8 ^{O}C /Km). The accumulation of sediments in a basin is a result of the interaction between subsidence rate, sediment influx, and the height of the water column (Allen and Allen, 2005). The sedimentation rate can be calculated by measuring the sedimentary succession, which was deposited over a period of time, taking into consideration the time of erosion and/or non-deposition. Compaction and decompaction is set as according to the lithology type within the PetroMod-1D software. Therefore, the temporal deposition of each lithostratigraphic unit was included to determine the rate of subsidence and sedimentation throughout the course of the geological timeline (Table. 1).

According to earlier studies of (Guiraud and Bosworth, 1999; Abd El Gawad et al.,2019; Edress et al., 2021; Passey et al., 2010), the vitrinite reflectance measurements and the corrected (Bottom Hole Temperature (BHT) for the modeled well were both used to calibrate the assumed heat flow through time. The geothermal gradient values exhibit a consistent pattern of steady increase with increasing depth and burial (Suggate, 1998).

Table 1. Tops, bottoms, thicknesses and ages of the modelled subsurface units in the Imhotep W-1X well, Matruh Basin.

Well	**Imhotep-W-1X**		
Layer	**Top (m)**	**Base (m)**	**Thick (m)**
Marmarica	0	84	84
MOGRA	84	439	356
DABAA	439	855	416
APOLLONIA	855	949	94
KHOMAN	949	1143	194
AR_AB	1143	1379	237
AR_CDE	1379	1600	221
AR_F1-G	1600	1932	332
BAH	1932	2116	183
KHARITA	2116	2600	485
DAHAB	2600	2624	23
Alamein	2624	2703	79
AEB_1	2703	2853	151
AEB_3A	2853	3057	203
AEB_3E	3057	3160	103
AEB_3G	3160	3440	280
AEB_4	3440	3574	133
AEB_5	3574	3967	394
AEB_6	3967	4060	93
MASAJID	4060	4306	246
ZAHRA	4306	4371	66
U.SAFA	4371	4594	223
Kabrit	4594	4605	11
L.SAFA	4605	4794	190
Ras Qattara	**N/A**		

4. Results and Interpretaion

4. 1.Kerogen Type and Organic richness

Kerogen types of the Khatatba shale examined rock samples that deposited in deltaic and inner shelf environments are determined by the Rock-Eval pyrolysis geochemical analysis using a plot of hydrogen index (HI) and oxygen index (OI) data on a pseudo Van Krevelen diagram (Van Krevelen, 1982; Dembicki, 2009). Both OI versus HI and T_{max} versus HI plots show that the Lower and Upper Safa and Zahra members of the Khatatba Formation have a dominantly gas-prone kerogen type III (Figs. 6A) having HI values > 50 mg HC/g TOC. The values of the T_{max} temperature range between 458 and 480 °C and have an average value of 471 °C (Figs. 6, 7B). This indicates that the Khatatba Formation entered the late mature (upper oil window to postmature wet gas/condensate) stage according to (Peters and Cassa, 1994; Baskin, 1997). On the other hand, the measuring of

organic richness, is expressed as the weight percentage of total organic carbon (wt% TOC_m), often carried out by elemental analysis or pyrolysis. Here in, the measured total organic carbon will be denoted as wt% TOC_m to differentiate it from the estimated well log-based $TOC_{\Delta logR}$. Studies made by (Passey et al., 1990; Creaney and Passey, 1993; Peters et al., 2005) demonstrated that the TOC derived from the well log data offers a comprehensive range of TOC information. As a result, the use of geochemical and geophysical methodologies was used to determine quantitatively the organic abundance.

4.2. Measured TOC_m data

According to (Peters and Cassa, 1994; Baskin, 1997) the organic richness of shale intervals in the Lower Safa member is classified as fair to excellent, with a range of 1.05–1.59 and an average of 1.29 wt% TOC. The data indicates that presence of coaly shale layers, as seen in the mud log which have high TOC wt%. The organic richness of the Upper Safa member shale layers has a range from fair to very good, with values ranging from 0.91–3.07 wt% TOC (average 1.90 wt% TOC). The S2 parameter is used to measure how pyrolizable organic matter can generate hydrocarbons in terms of mg HC/g rock. Accordingly, it serves as a more accurate indicator of source rocks potential (Dembicki, 2009; Hart and Steen, 2015). The S2 data shows that the Lower and Upper Safa members as well as the Zahra nember have poor petroleum generation potential (0.38 to 1.96 mg HC/g rock). The intermediate section of the Lower Safa member have a range of petroleum generation potential from fair to excellent (4.51–27.43, avg. 15.97 mg HC/g rock) (Fig.7A, B). This can be recognized by the presence of coaly shale layers in this section.

4.3. Well log-based $TOC_{\Delta logR}$ data

Estimating the TOC from wireline logs is very useful in providing a continuous range of TOC data across the subsurface units. A study by (Ali, 2009) showed that the Barnett Shale in west Texas contains a mixture of different types of kerogen I, II, and III. The variation in the kerogen types suggests a possible scenario involving changing depositional environments during the 25 million years of Barnett Shale deposition. The TOC data derived from the ΔlogR technique showed a weak correlation with geochemically measured TOC_m because of the change in depositional environment was considered in that study to be unreliable. However, for the Khatatba Formation in the Western Desert of Egypt, using the Δlog R technique for estimating $TOC_{\Delta logR}$ from wireline log was successful and showed a 70% consistency with the measured TOC from the analyzed samples. The correlation following (Passey et al., 1990) reveals high correlation coefficient values for the Lower Safa (0.86) and Upper Safa (0.64) members (Fig. 8a). Therefore, the TOC data derived from the ΔlogR method is considered to be reliable. The agreement between the measured total organic carbon (TOC_m) data and the geophysicaly calculated $TOC_{Schmoker}$ data obtained by the approach in (Van Krevelen, 1982) study is notably consistent only for the shale samples (Fig. 8b).

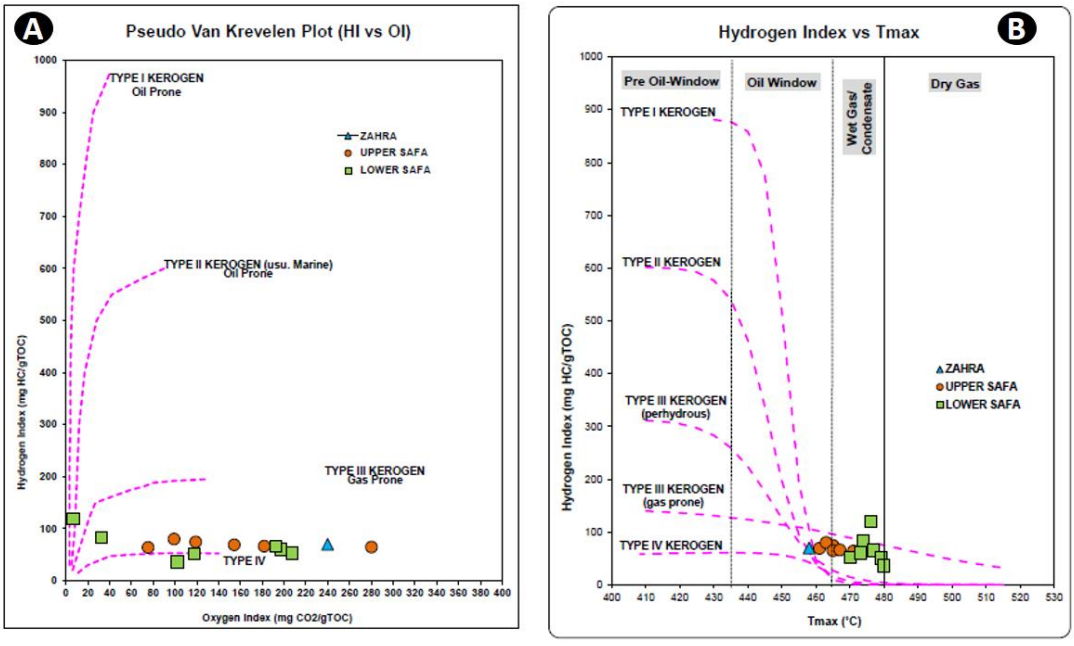

Fig. 6. (**A**): Plot of the oxygen index (OI) versus the hydrogen index (HI) data indicating a dominantly gas-prone kerogen type III in the Khatatba Formation. (**B**): Plot of T_{max} versus HI data indicating late mature (oil window) to early postmature (wet gas/condensate window) source rocks in the Khatatba Formation, the Imhotep W-1X well, Matruh Basin.

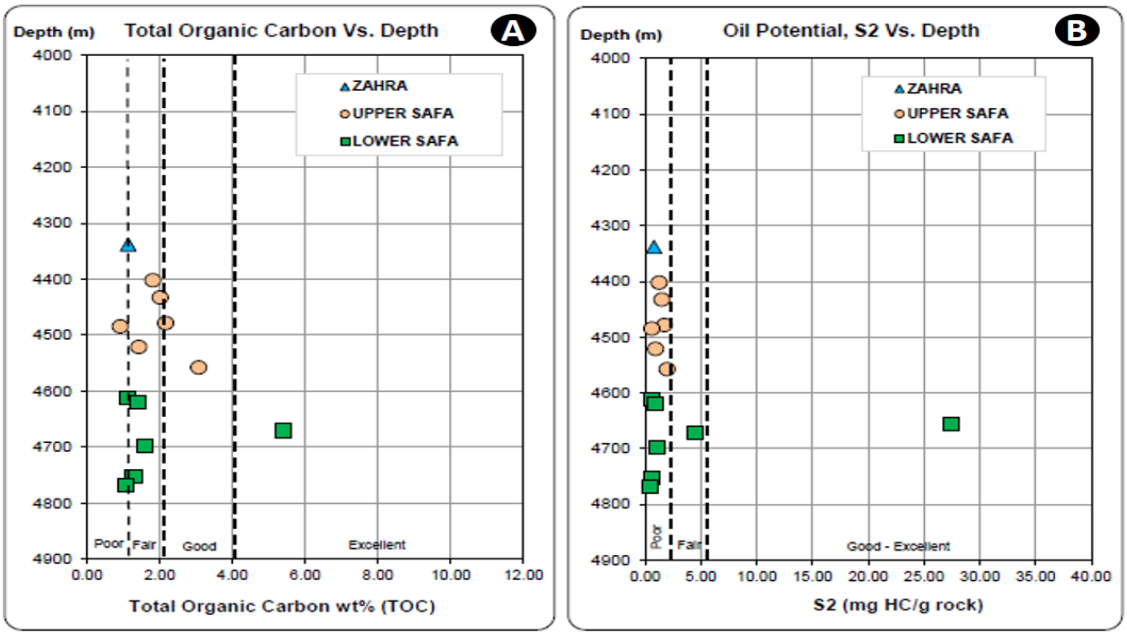

Fig 7. (A): Total organic carbon (TOC) wt% versus depth in meters show the shale intervals in the Lower Safa member are classified as fair to excellent, while the shale intervals of Upper Safa ranged from fair to good. **(B):** The S2 data shows that the Lower and Upper Safa members as well as the Zahra nember have poor petroleum generation potential.

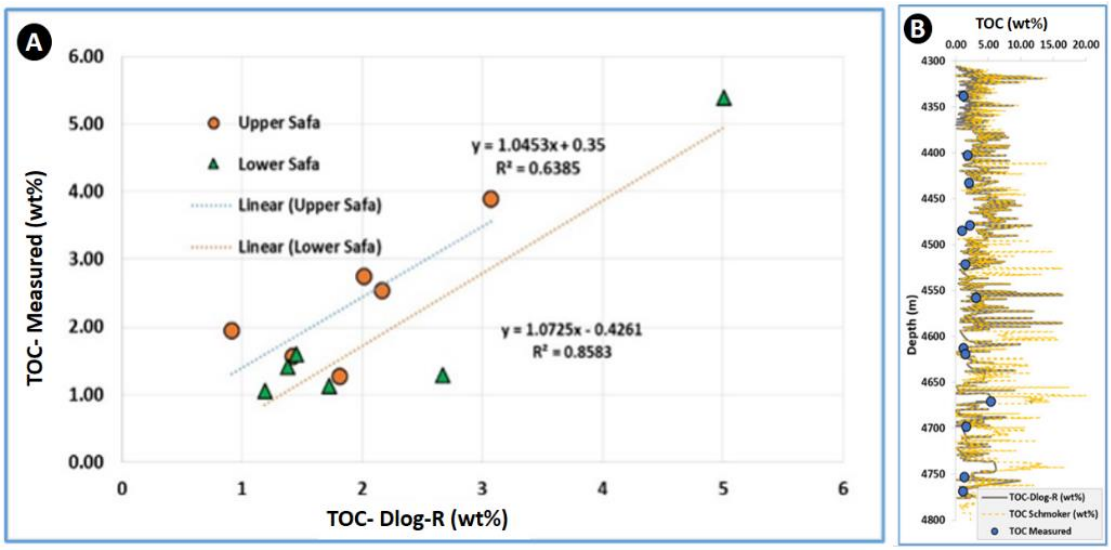

Fig. 8. (**A**): A cross-plot of the measured TOC and the estimated (ΔlogR) data showing high and moderate correlation coefficient values for the Lower Safa and Upper Safa members in the Imhotep W-1X well, respectively. (**B**): Correlation between the measured TOC data and the estimated $TOC_{Schmoker}$ data from the (Van Krevelen, 1982) method which shows good consistency for the shale samples only.

4.4. Geomechanics

The rock's brittleness increases proportionally with the magnitude of the brittleness index (BI). The analysis of the BI, in conjunction with the mineralogy logs along the Imhotep W-1X well, reveals that intervals characterized by elevated levels of quartz and calcite are more brittle compared to intervals with higher clay content, which display lower levels of brittleness and higher ductility. Furthermore, by separating organic rich shale intervals from the wireline logs using the (Passey et al., 2010) method, we observed that part of samples that contain high TOC and high GR values are more ductile, while the rest of samples that contain high TOC show same behavior as low TOC samples (Fig.9). Figure 9 illustrates that a TOC level greater than 2 wt% exhibits the highest dominance in the Upper Safa Member. This observation aligns consistently with a brittleness index beyond 40. The lower TOC content and non-TOC intervals show low GR (<60 API) and high BR (>40). The ductility of the rock increases with an

increase in the TOC content. However, most of the Upper Safa shale intervals are silty and contain quartz and carbonates, as confirmed by XRD (Table 3). They show a more ductile behavior. The high GR shale intervals with high TOC content show a ductile behavior, which can be justified based on the clay content. This behavior can also be monitored from the cross-plot of Poisson's ratio versus the Young's modulus, as illustrated in (Fig. 10).

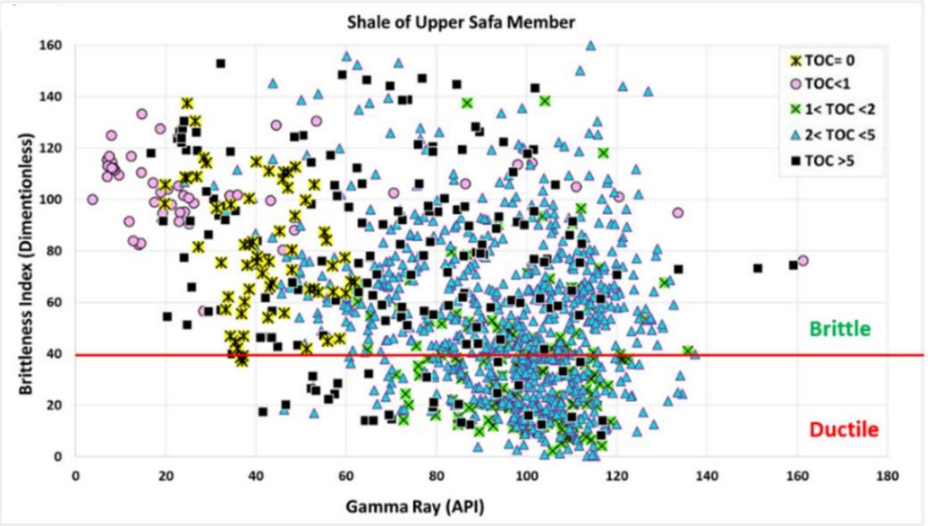

Fig. 9. Cross plot of GR (API) values versus the Brittleness Index of Upper Safa member shale intervals , show the relationship between the source rock maturity (TOC%) and brittleness index.

The ductile shale shows a high Poisson's ratio and a low Young's modulus. The inverse is true for the brittle shale. The shale of the Lower Safa Member **(**Fig. 10a) shows more brittle behavior than ductile**,** where the ductile intervals show high Poisson's ratio and low Young's modulus. The brittle intervals show high Young's modulus and low Poisson's ratio. In the Upper Safa Member (Fig. 10b), the ductile behavior of the shale, which corresponds to a high Passion's ratio and a low Young's modulus (R^2= 0.8572), is greater than the shale brittle behavior (R^2= 0.7944). The effect of clay minerals on the petrophysical properties of Lower and Upper Safa members are illustrated in (Table 2) , where the X-ray diffraction (XRD) examination of clay fractions collected from three samples within the Imhotep W-1X revealed that the Lower Safa Member contains a substantial proportion of kaolinite 33.27% in Sample 1. However, the Upper Safa Member has significant proportions of kaolinite, with Sample 11 containing around 47.42% and Sample 9 containing approximately 34.54%. The more ductile behavior of shale intervals in Safa members in the examined samples are consistent with high percentage of clay minerals content (Table 2) which accordingly show high Passion's Ratio and low Young's Modulus (Fig.10 a, b).

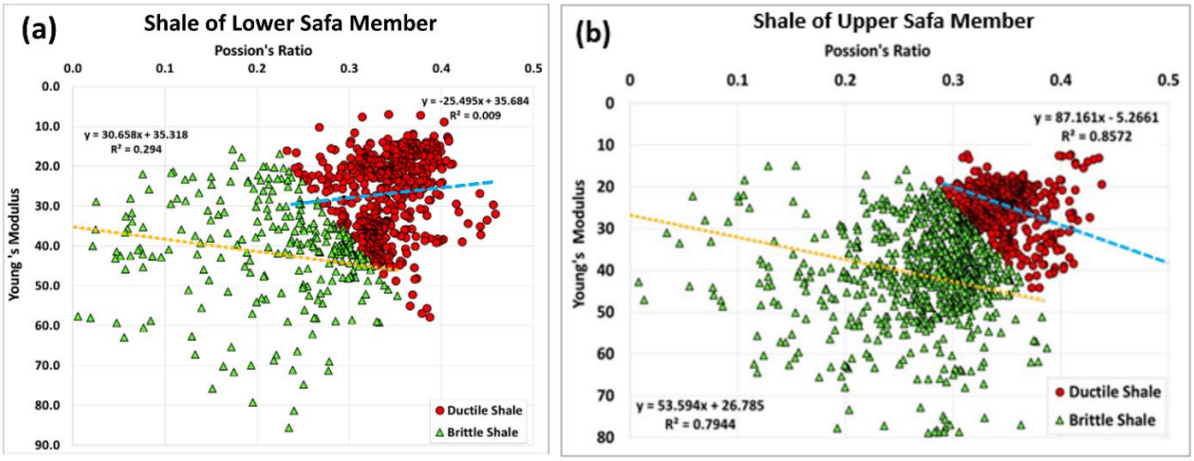

Fig.10. Young's modulus vs. Poisson's ratio of Lower Safa Member shale shows the variation in brittle and ductile behavior of the Khatatba Fm shale intervals. (**a**): Shale Intervals of Lower Safa member (**b**): Shale Intervals of Upper Safa member.

Table 2. XRD-clay fraction analysis for three samples from the Lower and Upper Safa members.

Sample.No	Sample.11	Sample.9	Sample.1
Depth (m)	4481.5	4524	4771
Unit	Upper Safa	Upper Safa	Lower Safa
Lithology	Silty Shale	Argillaceous Siltstone	Argillaceous Siltstone
Clay Min./ (Content %)	65.06	57.63	70.7
S/II	11.24	18.83	35.12
II (Illite)	2.1	5.2	1.3
Kaolinite	47.42	34.54	33.27
Chlorite	4.3	----	1.01
Non Clay Min (Content%)	33.78	42.37	29.29
Sand	8.18	12.78	8.25
Feldspar	0.27	0.488	
Gypsum	-----	-----	-----
Anhydrite	-----	8.62	------
Calcite	9.1	9.7	14.02
Dolomite	-----	-----	-----
Siderite	16.23	6.27	5.16
Pyrite	------	-----	1.86
Total	100	100	100

4.5. Modelling of the Matruh Basin

1D-burial history modelling at the location of the Imhotep W1-X well shows the burial history, sedimentation rate, time and depth to the oil and gas windows. It also provides valuable information about the basin's history (Waples, 1985; Ali and Fagelnour, 2023). The utilization of the PetroMod-1D program was employed for the purpose of constructing the burial history and calibrating the maturation model. The highest documented paleowater depth, measuring 600 m, occurred near the end of the Cretaceous period, around 69 Ma ago. Conversely, the North Western Desert experienced uplift during the Paleocene (Fig. 11a). The estimation of the sediment-water interface temperature (SWIT) is derived from the paleowater depth and the present geographic latitude, namely 30˚ north. The SWIT (Fig. 11b) reached its peak at 29˚C during the period from Early to Late Cretaceous (96-212 Ma).

Conversely, the lowest documented value of the SWIT was 14.7˚C, observed towards the end of the Cretaceous at 69.1 Ma. The heat flow value used in this study ranged between 40 and 75 mW/m^2 (Fig. 11c), which is characteristic of most rift basins in the north Western Desert of Egypt (Abd El Gawad et al., 2019). Figures 10a and 10b display the computed profiles of maturity and temperature gradient for the Imhotep W1-X well, respectively. The measured VR_o% in the Imhotep W-1X well (Fig. 12a) matches well with the predicted maturity curve. Also, the calculated temperature gradient matches the one obtained from BHT (Fig. 12b), which means the thermal model is well-calibrated. The age and temperature gradient curves exhibit a progressive increase as the depth of burial increases, which plays a significant role in the temporal transformation of organic matter into hydrocarbons (Galhom et al., 2022; Ali and Fagelnour, 2023).

The sedimentation rate model of the Imhotep W-1X well shows four major depositional cycles, each of which ends with a marine transgression. Two maximum sedimentation rates occurred: one in the first cycle (Jurassic rifting) and the other in the third cycle (Early Cretaceous rifting). The maximum sedimentation occurred during rift initiation, where source rocks accumulated at the base (i.e., Upper and Lower Safa, and AR-F1 to G members) **(**Fig. 13**).** The first cycle of the sedimentation rate model was initiated during the Jurassic rifting and led to the deposition of shales, sandstones, and siltstones of the Upper and Lower Safa members, with a high sedimentation rate of from 200 to 330 m/Ma. This high rate of deposition is related to rifting, where the subsidence rate increased, and shales formed the main source rocks at the base of the sedimentary basin (Bosworth et al., 2015).

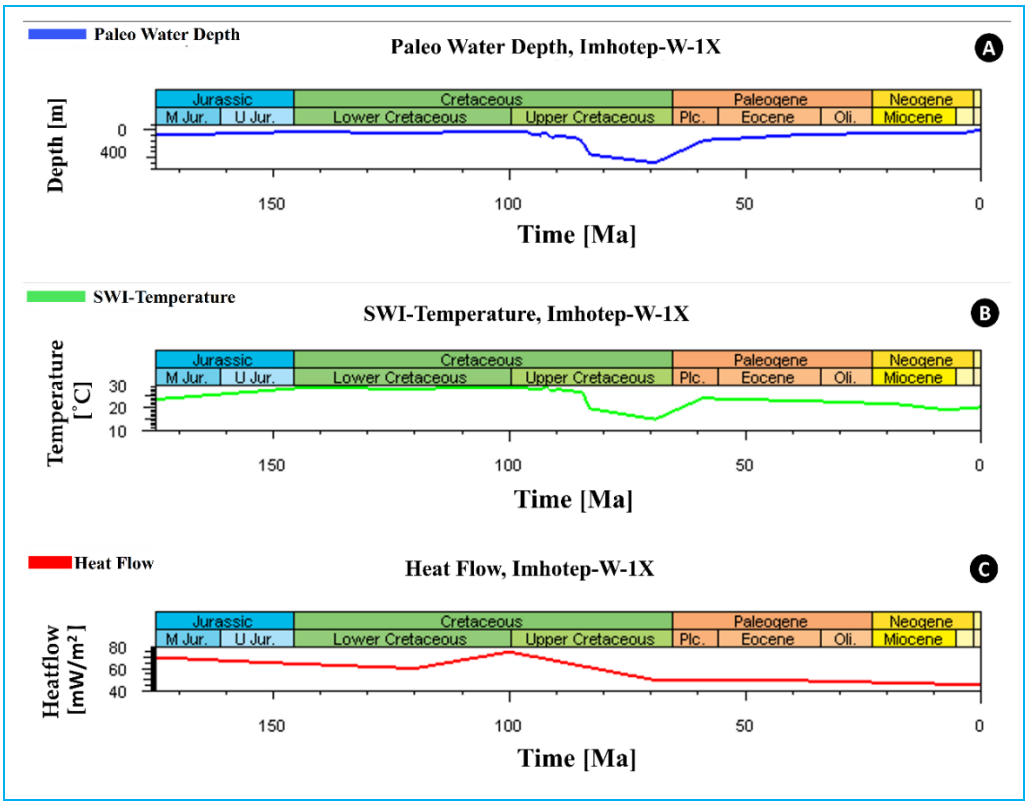

Fig. 11. The boundary conditions for the Imhotep W1X well are (A) paleowater depth, (B) sediment water interface temperature, and (C) heat flow.

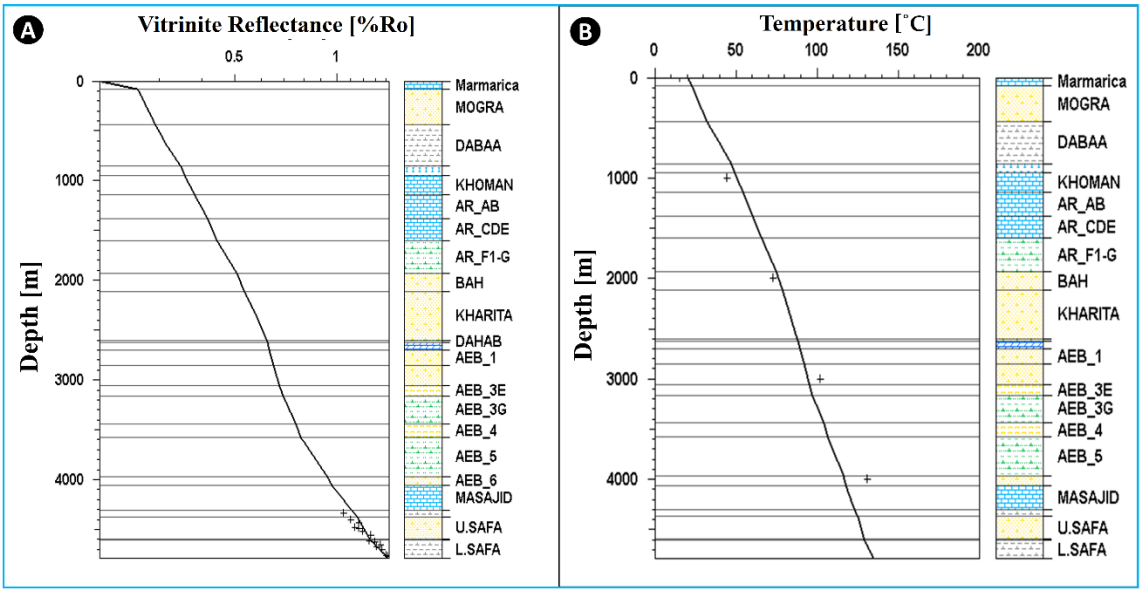

Fig.12. Computed profiles of maturity and temperature gradient for the Imhotep W1-X well (**A**) the maturity curve and measured vitrinite reflectance, and (**B**) the calculated and measured temperature gradient.

The deposition of the transgressive marine limestone of the Late Jurassic Masajid Formation marked the end of this cycle (Keeley et al., 1990). The second cycle started in the Early Cretaceous with the deposition of the Alam El Bueib (AEB) clastics and ended with the deposition of the carbonates of the Alamein Formation during a marine transgression. The maximum sedimentation rate recorded in this cycle was around 160 m/Ma, where rifting and

subsidence continued with a lower sedimentation rate (Fig. 13). The third cycle was initiated by a major rifting phase in the Late Cretaceous, when the water depth was at its maximum (up to 600 m) and the deep marine shales and limestones of the Abu Roash Formation were deposited.

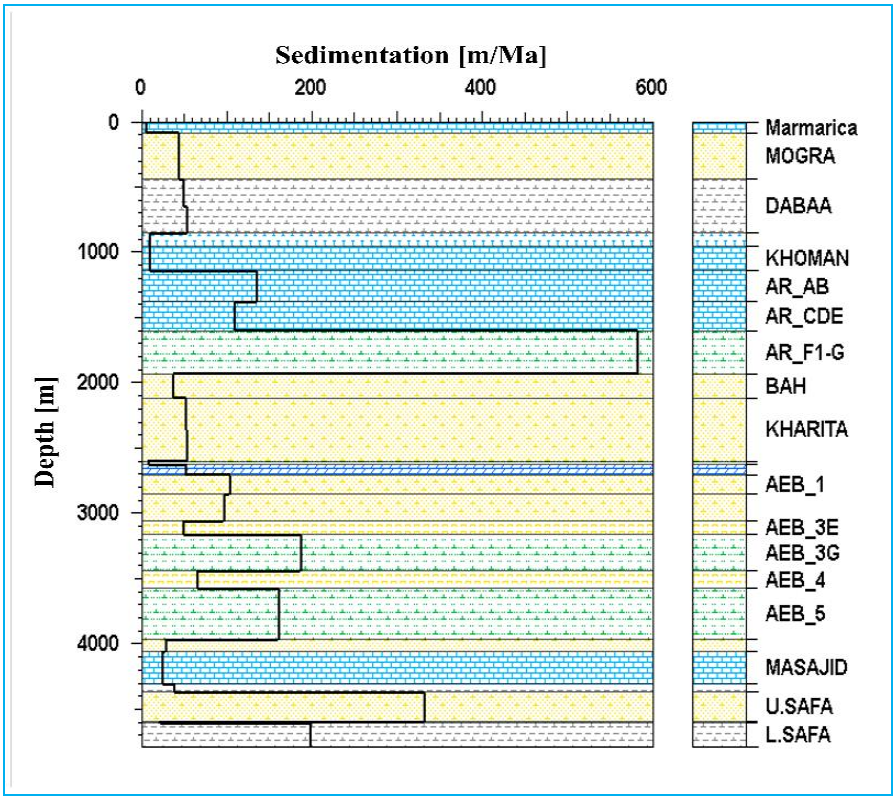

Fig.13. The sedimentation rate of Imhotep W-1X well in the Matruh Basin.

4.6. Burial and maturity histories of the Imhotep W-1X well in the Matruh Basin

The burial history modelling constructed by PetroMod-1D software used the kinetic model of (Sweeney and Burnham, 1990).to study the source rock maturity in Matruh Basin. The model indicates two main rifting phases (Fig. 14), one occurring in the Middle Jurassic (~ 173–170 Ma) and the other occurring in the Late Cretaceous (~ 93–92 Ma). The Late Cretaceous to Early Paleogene (~ 60–58 Ma) was characterized by a major uplift phase due to tectonic inversion. During the first phase of tectonic subsidence due to Jurassic rifting, the basin was characterized by a fluvial, near-shore to shallow marine setting (~ water depth 30–61 m), where fluvial sandstones, siltstones, and shallow marine shales and limestones were deposited. This is clearly noted in the shale source rocks of the Lower Safa and Zahra members (Ali and Fagelnour, 2023) and the sandstone reservoir rocks of the Upper Safa Member (Fig. 14). Subsidence continued during the Early Cretaceous and was characterized by the fluvial deposits of the Alam El Bueib Formation (Neocomian Phase) and interbedded by several shallow marine shales and carbonates layers (Fagelnour et al., 2019; Ali and Fagelour, 2023). This was followed by the deposition of the carbonates of the Aptian Alamein Formation, marine shales, and siltstones of the Dahab Formation, and ended with the fluvio-deltaic sandstones of the Kharita Formation. The end of the Early Cretaceous was characterized by a major unconformity, where argillaceous sandstones and siltstones of the Late Cretaceous (Cenomanian) Bahariya Formation were deposited in nearshore to shallow marine environments. The Late Cretaceous was characterized by a higher rate of subsidence with a deposition in a deep marine setting, where water depth ranged from (~ 457 to 573 m). This led to the deposition of the deep marine limestones and shales of the Abu Roash Formation (Ali and Fagelour, 2023). The end of the Cretaceous–Early Paleogene (60-58 Ma) was characterized by regional unconformity in the North Western Desert of Egypt due to uplift and erosion, followed by the deposition of limestones of the Apollonia Formation, shales of the Dabaa Formation, and sandstones of the Moghra Formation. According to Sweeny and Burnham's (1990) applied method, the color code legend of the burial history in Fig. 14 shows that the vitrinite reflectance values gradually increased, starting with blue (the immature zone) and ending with yellow (the overmature zone).

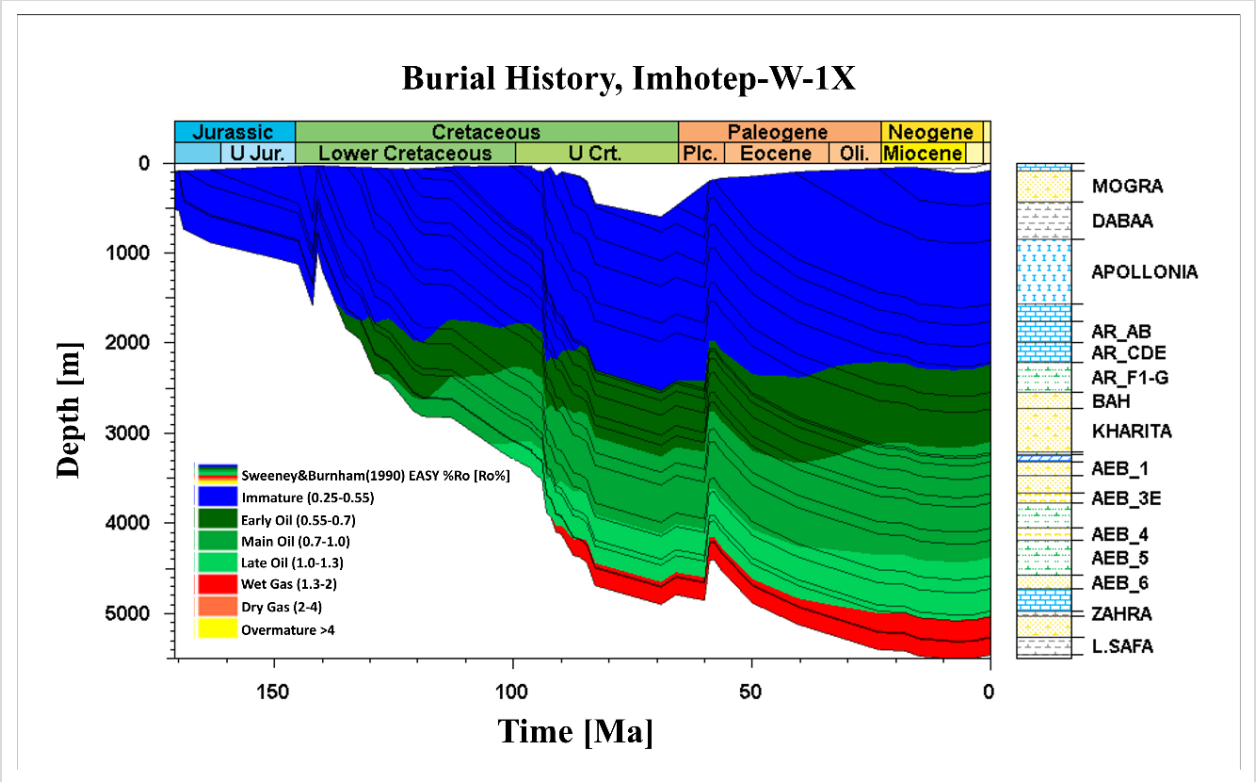

Fig.14. The burial history of the Imhotep W-1X well in the Matruh Basin.

The whole cycle ended with the deposition of the great limestone plateau of the Marmarica Formation, which covers most of the North Western Desert of Egypt (Sultan and Halim, 1988; Said, 1990). These phases of tectonic subsidence and inversion were responsible for the deposition of the main reservoir and source rocks and the structural traps formed during the Mesozoic period in the Matruh Basin. As a result of deposition and later burial of the Khatatba Formation, the organic-rich deposits were transformed into oil and/or gas (Tissot and Welte, 2013). Based on the previously constructed burial history model (Fig. 14), the onset of oil generation at (VR_o% of 0.70%) occurred in the Early Cretaceous period (~ 115–116 Ma), while the onset of wet gas generation at (VR_o% 1.30) began in the Late Cretaceous (~ 95 Ma). On the other hand, the depth at which the main oil window is began at 2941 m, and that of the wet gas window is located at 3990 m.

4.7. Hydrocarbon Expulsion Modeling of Matruh Basin

The amount of hydrocarbon generated and expelled (oil and gas) was evaluated based on the transformation ratio (TR) and kerogen type (Abd El Gawad et al., 2019; Sweeney and Burnham, 1990) The transformation ratio is defined as the ratio of the number of generated hydrocarbons to the total amount of hydrocarbons that the kerogen is capable to generate. The transformation ratios increase with increasing maturity and were used to predict the timing of petroleum generation and expulsion (Waples, 1985). The transformation ratio (TR) or the production index (PI) is calculated from the following equation:

TR (PI) = S1/ (S1+S2) [Waples, 1985], where: S1 refers to the free or distillable hydrocarbons which are available for migration and S2 refers to hydrocarbons generated from kerogen upon pyrolysis.

Expulsion was modelled to start at a transformation ratio (TR) of 10%. Expelled early oil, peak oil, and late oil windows are defined at TRs ranging from 10 to 25%, 25 to 50% and 50 to 80% respectively. More than 80% include the beginning of wet gas and condensate generation (Hantschel and Kauerauf,2009; Hakimi et al., 2018). Kerogen type, total organic carbon (wt% TOC), and hydrogen index (HI) for the studied Zahra and Lower Safa shale source rocks are listed in Table 3. The hydrocarbon generation and expulsion history based on the calculated TR and modelled maturity of the source rocks in the study well are shown in Table 4 and Figure 14.

Table 3. Kerogen type, total organic carbon (TOC %), and hydrogen index (HI) for the studied Zahra and Lower Safa shale source rocks in and Imhotep W-1X well.

Well	Unit	Kerogen type	HI (mg HC/ g TOC)	TOC %
Imhotep-W-1X	Zahra	Mixed III/ II	70	1.1
	Lower Safa	Mixed III/II	84	5.4

The first stage of hydrocarbon generation of the Zahra Member shale in the Imhotep W-1x well occurred during the Late Cretaceous at 129-112 Ma ago. This stage is the early phase of oil generation without any expulsion. The TR of the Zahra shale varied from 26 to 36% during this stage with the computed vitrinite reflectance (VR_o) being 0.55-0.7%. The second stage (112-91 Ma) in the Late Cretaceous is the main phase of the oil generation with TR 36 to 50% and calculated VR_o of 0.7–1%. The third stage is the late oil stage with TR 50 to 65% and VR_o 1 to 1.3% occurred in the Late Cretaceous to Recent (87 to 0 Ma) (Table. 4 and Fig.15). The first stage of hydrocarbon generation of the Lower Safa Member shale in the Imhotep W-1x well occurred during the Early Cretaceous at 135-123 Ma. This stage is the early phase of oil generation without any expulsion. The TR of the Lower Safa shale varied from 26 to 36% during this stage with the computed vitrinite reflectance (VR_o) being 0.55-0.7%. The second stage (123-100 Ma) in the Early Cretaceous is the main phase of the oil generation with TR 36 to 50% and calculated VRo of 0.7-1%. The third stage is the late oil stage with TR 50 to 65% and VRo 1 to 1.3% occurred in the Early to Late Cretaceous (100 to 87.5 Ma). The fourth stage is the gas and condensate generation stage with TR from 65 to 100% and VRo 1.3 to 2% occurred in the Late Cretaceous to Recent (87.5 to 0 Ma) (Table. 4 and Fig. 15).

Table 4. The calculated TR and modelled VRo of the Khatatba Fm. source rocks in Imhotep W-1X well.

Fm./Unit	Onset oil generation				Main oil generation			
	TR %	VRo %	Time (Ma)	Age	TR %	VRo %	Time (Ma)	Age
Khatatba/ (Zahra)	26-36	0.55-0.7	129-112	Late Cretaceous	36-50	0.7-1	112-91	Late Cretaceous
Khatatba/ (Lower Safa)	26-36	0.55-0.7	135-123	Early Cretaceous	36-50	0.7-1	123-100	Early Cretaceous
Fm./Unit	**Late oil generation**				**Wet gas and condensate generation**			
Khatatba/ (Zahra)	50-65	1-1.3	91 -0	Late Cretaceous - Recent	65-100	None		
Khatatba/ (Lower Safa)	50-65	1-1.3	100-87.5	Early- Late Cretaceous	65-100	1.3-2	87.5-0	Late Cretaceous - Recent

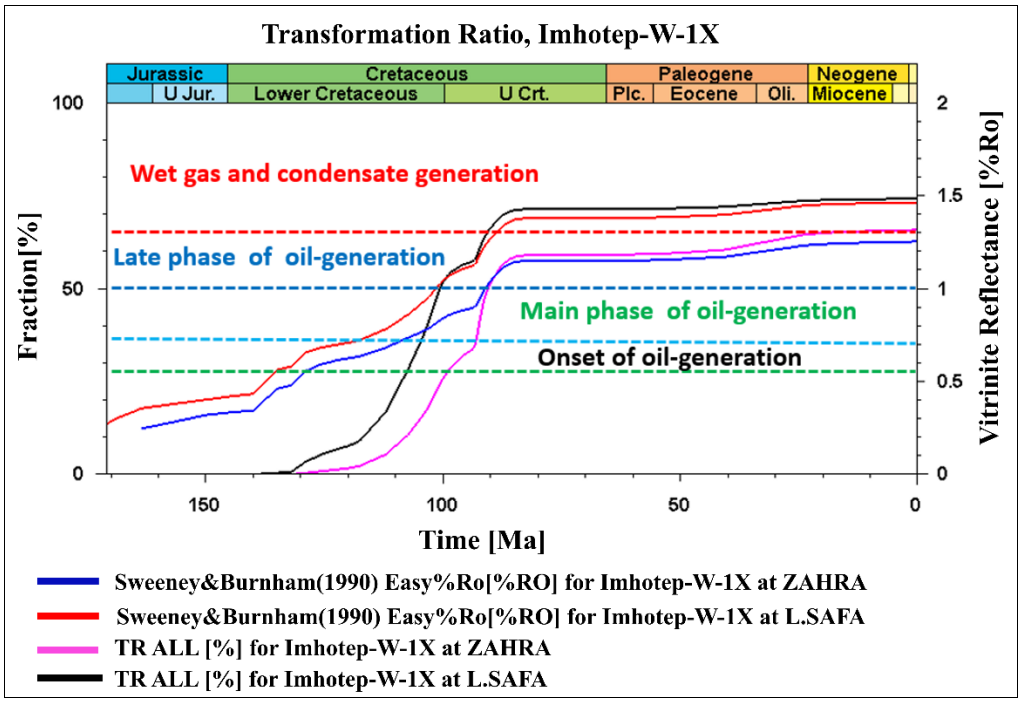

Fig. 15. Transformation ratio evolution with age and vitrinite reflectance versus time for Zahra member Shale and Lower Safa Shale, in Imhotep W-1X well.

4.8. The petroleum system of the Khatatba Formation in the Imhotep Field

The petroleum system includes all elements of petroleum generation and accumulation in a basin (Walters, 2006) These elements include source rocks, reservoir rocks, seal rocks, geological structures forming petroleum traps, and faults that act as conduits for hydrocarbons' migration (Peters and Cassa, 1994). The petroleum system events chart of the Imhotep W-1X well is shown in (Figure 16). The shale source rocks were deposited during the Middle Jurassic (~ 175–163 Ma) and include the Lower and Upper Safa and Zahra members. The sandstone reservoir rocks of the Ras Qattara Formation, Upper Safa, and AEB-6 members were deposited during the Early and Middle Jurassic and Early Cretaceous, respectively (~ 200–140 Ma). The shales and siltstones of the AEB-5 Member act as the main seal rock and were deposited during the Early Cretaceous (~ 140–135 Ma). The carbonates of the Kabrit Member and shale interbeds of the Safa Member act as secondary sealing rocks in the Imhotep W-1X well. The main structural traps were formed during the Jurassic–Early Cretaceous (~ 180–140 Ma) and the onset of oil generation, migration, and accumulation started in the Early Cretaceous (~ 125 Ma). The traps were formed during the Jurassic and Cretaceous rifting phases of the Matruh Basin and were later charged by petroleum through migration and accumulation, which is characteristic of all Mesozoic rift basins in the North Western Desert of Egypt (Taha, 1992; Radwan, 2023; Ali and Fagelnour, 2023; Attiya et al., 2023; Mahmoud et al., 2024; Ali et al., 2024).

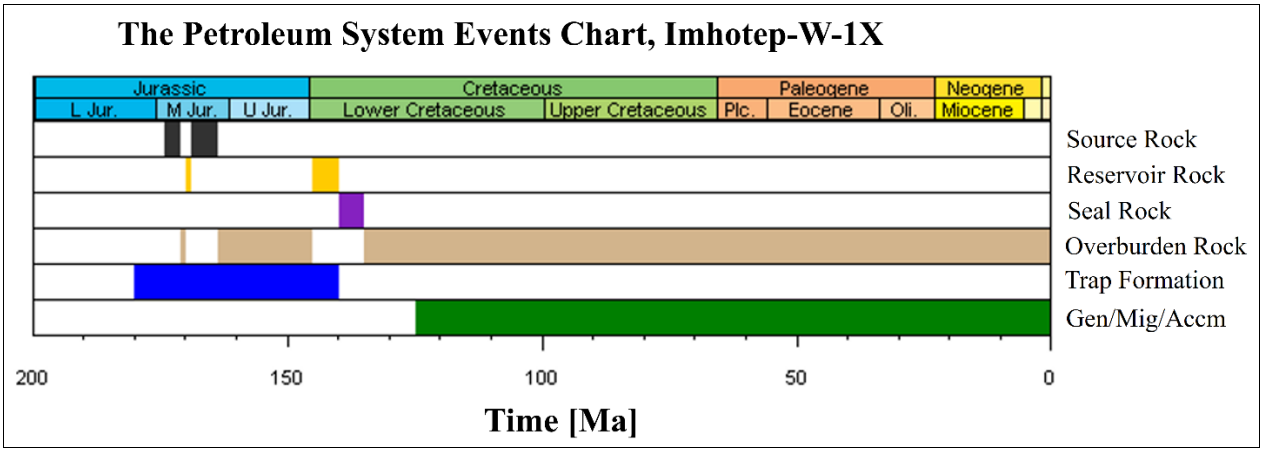

Fig. 16. The petroleum system event chart of the Imhotep W-1X well in the Matruh Basin

5. Discussion

Petroleum potential of the Khatatba Formation in the Imhotep W-1X well

The investigations made by (Ali, 2023) on the Khatatba Formation in the Matruh-5 and Matruh-6 wells showed that depositional and climatic conditions had a significant impact on the sedimentary facies, organic facies, and organic richness. The Khatatba Formation shows alternations between organic-poor coarse clastics and organic-rich shales and carbonates. The deposition of the organic-rich intraformational shale source rocks in marine prodelta environments of the Lower and Upper Safa members was related to the favorable sedimentological conditions. These were characterized by favorable reducing conditions, fair primary bio productivity, and relatively low terrigenous influxes brought to the basin during relatively semi-arid conditions. Deposition of the organic-lean coarse clastic reservoirs in tide-dominated brackish delta front and delta channel environments of the Lower Safa and Upper members was related to higher terrigenous inputs associated with a more humid climate and Tethyan Sea level falls during the Middle Jurassic.

Results of the current study indicate that the middle part of the Lower Safa Member shows excellent source rock potential due to high enrichment in carbonaceous material and coal layers accumulated under suboxic–anoxic conditions. However, the Upper Safa Member is characterized by thinner shale and thicker siltstone source rock interbeds, which were deposited in the energetic proximal delta front and delta channel settings and also contain gas-prone organic facies. The burial history construction along with the organic geochemical and petrographic data indicate that the maturation of the Khatatba Formation source rock intervals was driven by tectonic subsidence events, which were related to the Tethyan rifting (Guiraud et al., 2001; Bosworth and Tari, 2021; Ali and Fagelnour, 2023). The Khatatba Formation source rocks were brought by the Late Jurassic minor subsidence at shallow burial depths. The deposition of shale and siltstone seal rocks in the AEB-5 Member during the Early Cretaceous was followed by the late Early Cretaceous subsidence, which initiated the maturation of the Khatatba Formation source rocks. As a result, some oil was generated, migrated, and accumulated in the sandstone reservoirs of the Upper Safa Member of the

Middle Jurassic Khatatba Formation and the AEB-6 Member of the Lower Cretaceous Alam El Bueib Formation and trapped in the pre-existing Jurassic and Early Cretaceous structural traps. The Middle Jurassic Khatatba Formation's deeper burial depths, which were the result of the Late Cretaceous major subsidence, enhanced greatly the maturation process (Khalda, 2014). The continued deposition of thick overburden over the seal rocks brought the source rocks to deeper burial depths, which further enhanced their maturation by the Oligocene and resulted in the generation of wet gas and condensates.

Generally, the Lower and Upper Safa members of the Khatatba Formation show poor to fair gas generation potential, except for the carbonaceous shale and coal layers of the middle part of the Lower Safa Member, which show excellent organic richness and fair to excellent wet gas and condensate generation potential. According to the constructed basin model, the Khatatba Formation is in the late mature zone, resulting in the generation of oil and/or gas based on the Kerogen type which is mixed III/II, and it is capable of generating both oil and gas base on maturity level (whether oil or gas window). The AEB-6 is located in the main mature zone. However, AEB-6 produces gas because all source rocks contain mostly kerogen type-III with minor type-II. Thus, the area produces gas and condensate upon maturity. The produced gases from the AEB-6 reservoir are accompanied by condensate, which is consistent with the results of the basin model, which shows late oil window and postmature gas window stages.

In a worldwide context, Ali (2009) studied the XRD-determined clay mineral content of the Barnett Shale and found that this formation generally contains less than 30% clay minerals. Silica (clay to silt-size crystalline quartz) was by far the most dominant component of the Barnett Shale, where the increase in the silica content in the Barnett Shale made it more brittle and easier to fracture with drilling. However, the Khatatba Formation shows an increase in the percentage of clay mineral contents up to > 60%, which negatively affects its reservoir quality. Comparing the clay and non-clay mineral content data of the Woodford Formation and the Barnett Shale in west Texas basins to the Khatatba Fm, showed that the silica content of the Barnett Shale and Woodford Formation is higher than that of the Khatatba Formation. This improved the shale brittleness and allowed it to fracture more easily in the Texas basins.

From the above discussion, it is suggested that the Khatatba Formation in the Imhotep W-1X well shows *in situ* dual source and reservoir characteristics, which are related to the deposition of alternations of coarse clastic reservoirs and fine clastic and carbonate source rocks. These changes in the depositional environments are connected to the Middle Jurassic Tethyan Sea level changes and the development of more humid regional climatic conditions. On the other hand, the main source rocks in the Matruh Basin are believed to be the Middle Jurassic Khatatba Formation shales. Economically, in the Imhotep W-1X well, the Khatatba shales are not typical shale gas source rocks, and they are not thick enough where they occur as intraformational shale layers. Generated gas and oil are probably trapped in conventional stratigraphic and structural traps. Overall, the presence of hydrocarbons in several nearby wells shows the need for further investigations of the Khatatba Formation source rock potential**.** Therefore**,** integrating geomechanics, geochemical, and petrophysical analysis, along with elemental analysis, can help plan and optimize operations. The integration applied in this study can help define horizontal well orientation in the case of multi-well correlation, evaluate the suitability of particular zones in the formation for hydraulic fracturing, and measure the pressure required for hydraulic fracturing.

6. Conclusions

1) Integrated multi approaches such as organic/inorganic geochemical, and organic petrographic analyses were conducted for the Middle Jurassic Khatatba Formation in the Imhotep W-1X well, Matruh Basin, Northwestern Egypt, to investigate its petroleum potential. Results indicate that the Khatatba Formation shows obvious *in situ* dual source and reservoir characteristics. This is related to the alternations in sedimentation, which resulted in alternating deposition of organic-poor coarse clastic reservoirs during semi-humid conditions and deposition of organic-rich fine clastic and carbonate source rocks during semi-arid conditions.

2) The shallow marine source rocks are rich in late mature to early postmature (wet gas to dry gas windows) gas-prone organic facies, which sourced the juxtaposing intraformational coarse clastic reservoirs with gas and condensates.

3) Hydrocarbon charge at the location of the Imhotep W-1X well is believed to be sourced from the mature Khatatba shale source rock intervals, which encased the clastic reservoirs. These source rocks are presently thermally mature to generate mostly gaseous hydrocarbons, which is confirmed by the maturation proxies and actual shows in the mud log.

4) The thermal maturation of these source rocks was connected to the thermal and tectonically driven subsidence events, which were related to the Late Jurassic and Cretaceous Tethyan rifting.

5) The Lower Safa, Upper Safa, and Zahra members are shale-dominated in the prospect area. These shales form the top and lateral seals for the Imhotep W-1X well prospect accumulation. However, sealing is not anticipated to be a major problem.

6) The prospect area has direct access to mature source rocks within the studied part of the Matruh Basin, which contains the mature Middle Jurassic Khatatba Formation source rocks.

7) The varying petrophysical characteristics and geomechanical complications of the Upper and Lower Safa sandstone reservoirs necessitate studying other parts of the Matruh Basin to better understand their regional hydrocarbon production potential.

Acknowledgments:

The Authors are very grateful to the Egyptian General Petroleum Corporation (EGPC) and Khalda Petroleum Company for granting rock samples and well logging data for the Imhotep W-1X well. The 1st author is indebted to the Fulbright Scholarship for getting funds to support the analysis of XRD clay fraction. Authors are also grateful to Dr. Amr Deaf from Assuit University for his cooperation in analyzing the cutting samples by rock eval pyrolysis at Stratochem Services co.

Credit Author Statement:

The authors certify that they all contributed to the current article to be included as co-authors. Material preparation, data collection, proposal writing, and the approval process to use the data used in this research from the Egyptian General Petroleum Corporation (EGPC) were performed by the 1st author [Walaa A. Ali], who worked on the concept, design, laboratory preparation of samples, data analysis, drawing illustrations, tabulating data, and finally writing and revision of the manuscript. The 2nd author [Mohamed Fagelnour] worked on data acquisition, analysis, drawing, and confirming the illustrations of the basin model section in this manuscript.

Declaration of competing interest:

The authors affirm that they do not possess any identifiable conflicting financial interests or personal ties that could have potentially influenced the findings presented in this manuscript.

References

Abd El Gawad, E.A., Ghanem, M.F., Lotfy, M.M., Mousa, D.A., Temraz, M.G., & Shehata, A.M., (2019). Burial and thermal history simulation of the subsurface Paleozoic source rocks in Faghur Basin, north Western Desert, Egypt: Implication for hydrocarbon generation and expulsion history. Egypt. J. Pet. 28, 261–271.

Ali, W.A., (2009). Lithofacies, depositional environment, burial history, and calculation of organic richness from the wireline logs: a study of Barnett Shale in the Delaware Basin, Pecos Co., West Texas, and comparison with the Barnett Shale in the Fort Worth Basin (Doctoral dissertation).

Ali, W. A., & Fagelnour, M., (2023). Burial and thermal history simulation of the Middle Jurassic source rocks in Matruh basin, north Western Desert, Egypt, (2023). Delta Journal of Science 47(1), 171-191.

Ali, W. A., (2023).Depositional environment and paleoclimate of the Middle Jurassic sedimentary rocks in Matruh Basin, Northwestern Desert, Egypt. Egypt. J. Geol. 67(1), 299-319 (2023).

Ali, W.A., Deaf, A.S.,& Mostafa, T., (2024). 3D geological and petrophysical modeling of Alam El-Bueib formation using well logs and seismic data in Matruh field, northwestern Egypt. Sci. Rep. 14, 6849.

Ali, W.A. (2024).The Reservoir potential of Middle Jurassic sedimentary deposits in the Imhotep Field, Matruh Basin, North-Western Egypt. FSRT, 2024, 9, 35-47

Allen, P.A., & Allen, J.R., (2005). Basin analysis: Principles and Applications. 2nd Ed., Oxford, England: Blackwell Science Publication, 373–318.

Attiya, A.S., Kassab, M.A., Salem, T.M., & Abbas, A.E., (2023). Source rock evaluation and burial history modeling of the Middle Jurassic Khatatba Formation in the West Kanayes Concession of Matruh Basin, North Western Desert, Egypt. Egypt. J. Chem., 66, 71-85.

Baskin, D.K., (1997). Atomic H/C ratio of kerogen as an estimate of thermal maturity and organic matter conversion. AAPG Bulletin 81, 1437–1450.

Bosworth, W., Drummond, M., Abrams, M., & Thompson, M., (2015). Jurassic rift initiation source rock in the Western Desert, Egypt – relevance to exploration in other continental rift systems. In: Petroleum Systems in “Rift” Basins, 34th Annual GCSSEPM Foundation Perkins Rosen Research Conference, Houston, 13–16.

Bosworth, W., & Tari, G., (2021). Hydrocarbon accumulation in basins with multiple phases of extension and inversion: Examples from the Western Desert (Egypt) and the western Black Sea. Solid Earth Discussions 12, 59–77.

Bunaciu, A.A., UdriŞTioiu, E.G., & Aboul-Enein, H.Y., (2015). X-ray diffraction: instrumentation and applications. Critical reviews in analytical chemistry, 45, 289-299.

Creaney, S., & Passey, Q.R., (1993). Recurring patterns of total organic carbon and source rock quality within a sequence stratigraphic framework. AAPG Bulletin 77, 386–401.

Crain, E.R., & Holgate, D., (2014). A 12-step program to reduce uncertainty in kerogen-rich reservoirs. GeoConvention, 12-16.

Delle Piane, C., Bourdet, J., Josh, M., Clennell, M.B., Rickard, W. D., Saunders, M., & Raven, M. D., (2018). Organic matter network in post-mature Marcellus Shale: Effects on petrophysical properties. AAPG Bulletin, 102, 2305-2332.

Dembicki, H., (2009). Three common source rock evaluation errors made by geologists during prospect or play appraisals. AAPG Bulletin 93, 34–356.

Diab, A. I., & Khalil, H. M. (2021). Quantitative assessment of the tight gas reservoirs in the Obaiyed field, Shushan Basin, NW Egypt. NRIAG Journal of Astronomy and Geophysics, 10(1), 320-332.

Edress, N.A.A., Darwish, S., & Ismail, A., (2021). Geochemical characterization of the source rock intervals, Beni-Suef Basin, West Nile Valley, Egypt. Open Geosciences 13, 1536–1551.

EGPC, (1992). Western Desert, Oil and Gas Fields, A comprehensive Overview. EGPC, 11th Petroleum Exploration Production Conference, Cairo, Egypt, 431.

El-Shorbagy, A. I., Mousa, D. A., Makled, W. A., & El Din, M. Y. Z., (2023). Sequence stratigraphic modeling and organic matter distribution of Jurassic deposits in the Imhotep Field, Matruh Basin, Western Desert, Egypt. Neues Jahrbuch für Geologie und Paläontologie-Abhandlungen, 215-234.

Fagelnour, M., Gamil, I., El Toukhy, M., Gharieb, A., & Saad, H., (2019), March. Source rock potentiality, basin modeling, and oil to source correlation in Northern Shushan Basin, Western Desert, Egypt. In Offshore Mediterranean conference and exhibition, (OMC-2019). OMC.

Galhom, T., Mann, P., & Rudolph, K., (2022). Jurassic–recent stratigraphy, structure, and hydrocarbon potential of the Mesozoic–Cenozoic rifted-passive margin of the Tarfaya–Dakhla basin of southern Morocco. Mar. Pet. Geol. 139:105626.

Gentzis, T., Carvajal, H., Deaf, A., & Tahoun, S.S., (2018). Multi-proxy approach to screen the hydrocarbon potential of the

Jurassic succession in the Matruh Basin, north Western Desert, Egypt. Int. J. Coal Geol. 190, 29–41.

Guiraud, R., Issawi, B., Bosworth, W., Ziegler, P.A., Cavazza, W., Robertson, A.H.F., & Crasquin-Soleau, S., (2001). Phanerozoic history of Egypt and surrounding areas. Peri-Tethys Memoir 6, 469–509.

Guiraud, R., & Bosworth, W., (1999). Phanerozoic geodynamic evolution of north–eastern Africa and the north–western Arabian platform. Tectonophysics 315, 73–108.

Hakimi, M.H., Mohialdeen, I.M., Al Ahmed, A.A., & El Nady, M.M., (2018). Thermal modeling and hydrocarbon generation of the Late Jurassic-Early Cretaceous Chia Gara Formation in Iraqi Kurdistan region, northern Zagros Fold Belt. Egypt. J. Pet., 27, 701-713.

Hantschel, T., & Kauerauf, A. I., (2009). Fundamentals of basin and petroleum systems modeling. Springer Science & Business Media.

Hassan, M.S., & Baioumy, H.M., (2006). Structural and chemical alteration of glauconite under progressive acid treatment. Clay Miner., 54, 491-499.

Hart, B.S., & Steen, A.S., (2015). Programmed pyrolysis (Rock-Eval) data and shale paleoenvironmental analyses: A review. Interpretation, 3,.SH41–SH58.

Jaeger, J.C., Cook, N.G., & Zimmerman, R., (2009). Fundamentals of rock mechanics. John Wiley & Sons.

Keeley, M.L., Dungworth, G., Floyd, C.S., Forbes, G.A., King, C., McGarva, R.M., & Shaw, D., (1990). The Jurassic System in northern Egypt: I. Regional stratigraphy and implications for hydrocarbon prospectivity. J. Pet. Geol. 13, 397–420.

Khalda Petroleum Company, (2014). Final Report and Composite log of the Imhotep W-1X well (Cairo).

Knippel, E.P., Xiong, Q., Vargas, A.P.V., & Hampton, J. C., (2023). Measurements of elastic properties and their dependencies within a damage mechanics workflow. Rock Mechanics Bulletin, 2, 100083.

Mahmoud, M.M.K., Abu El-Ata, A.S., & Lala, A.M, (2024). Petrophysical Evaluation of Khatatba Formation in El-Obaiyed Area, Northern Western Desert, Egypt. Appl. Geophys., 23, 1-22.

Metwalli, F.I., Pigott, J.D., Ramadan, F.S., El-Khadragy, A.A., & Afify, W.A., (2018). Alam El Bueib reservoir characterization, Tut oil field, North Western Desert, Egypt. Environ. Earth Sci. 77, 1–21.

Meyer, B.L., & Nederlof, M.H., (1984). Identification of source rocks on wireline logs by density/resistivity and sonic transit time/resistivity crossplots. AAPG bulletin, 68, 121-129.

Fello, N.M., Deaf, A.S., & Leila, M., (2024). Petroleum Geology of North Africa. In: Z. Hamimi et al. (eds), The Geology of North Africa, Regional Geology Reviews,

Passey, O.R., Moretti, F.U., & Stroud, J.D., (1990). A practical modal for organic richness from porosity and resistivity logs. AAPG Bulletin 74, 1777–1794.

Passey, Q. R., Bohacs, K. M., Esch, W. L., Klimentidis, R., & Sinha, S., (2010). From oil-prone source rock to gas-producing shale reservoir–geologic and petrophysical characterization of unconventional shale-gas reservoirs. SPE IOGCEC, SPE-131350.

Peters, K.E., & Cassa, M.R., (1994). Applied source rock geochemistry. In: Magoonand, L. B., Dow, W. G. (Eds.), the petroleum system from source to trap. AAPG Bulletin, 93–120.

Peters, K.E., Walters, C.C., & Moldowan, J.M., (2005). The Biomarker Guide, 2nd ed., Cambridge University Press, Cambridge.

Perez Altamar, R., & Marfurt, K., (2014). Mineralogy-based brittleness prediction from surface seismic data: Application to the Barnett Shale. Interpretation, 2, T255-T271.

Pickel, W., Kus, J., Flores, D., Kalaitzidis, S., Christanis, K., & Cardott, B.J., et al., (2017). Classification of liptinite – ICCP System 1994. Int. J. Coal Geol, 169, 40–61.

Pillot, D., Deville, E., & Prinzhofer, A., (2014). Identification and quantification of carbonate species using Rock-Eval pyrolysis. Oil & Gas Science and Technology – Revue d'IFP Energies nouvelles 69, 341–349.

Radwan, A.E., (2023). Western desert petroleum system: New exploration opportunities and challenges. The Phanerozoic Geology and Natural Resources of Egypt, PP.691-717.

Rickman, R., Mullen, M., Petre, E., Grieser, B., & Kundert, D., (2008). A practical use of shale petrophysics for stimulation design optimization: All shale plays are not clones of the Barnett Shale. In SPE Annual Technical Conference and Exhibition. (SPE-115258).

Rolfs, S. A., (2015). Integrated geomechanical, geophysical, and geochemical analysis of the Bakken Formation, Elm Coulee field, Williston Basin, Montana. 2015-Mines Theses & Dissertations.

Rowe, H., S. Ruppel, S. Rimmer, & R. Loucks, (2009). Core-based chemostratigraphy of the Barnett Shale, Permian Basin, Texas: GCAGS, v. 59, p. 675-686.

Said R., (1990). The Geology of Egypt. Balkema-Rotterdam-Brookfield.

Schmoker, J.W., & Hester, T.C., (1983). Organic carbon in Bakken Formation United States portion of Williston Basin. AAPG Bulletin 67, 2165–2174.

Shalaby, M.R., Hakimi, M.H., & Abdullah, W.H., (2014). Petroleum system analysis of the Khatatba formation in the Shoushan basin, north western desert, Egypt. Arab. J. Geosci., 7, 4303-4320.

Sohail, G. M., Hawkes, C. D., & Yasin, Q., (2020). An integrated petrophysical and geomechanical characterization of Sembar Shale in the Lower Indus Basin, Pakistan, using well logs and seismic data. J. Nat. Gas Sci., 78, 103327.

Schön, J.H., (2015). Physical properties of rocks: Fundamentals and principles of petrophysics. Elsevier.

Schlumberger, (1995). Well evaluation conference, 56–71

Suggate, R.P., (1998). Relations between depth of burial, vitrinite reflectance and geothermal gradient. Journal of Petroleum Geology 21, 5–32.

Sweeney, J. J., & Burnham, A. K. (1990). Evaluation of a simple model of vitrinite reflectance based on chemical kinetics. AAPG bulletin, 74(10), 1559-1570.

Sýkorová, I., Pickel, W., Christanis, K., Wolf, M.,Talor, G.H., & Flores, D., (2005). Classification of huminite – ICCP system 1994. Int. J. Coal Geol, 62, 85–106.

Sultan, N., & Halim, M.A., (1988). Tectonic framework of northern Western Desert, Egypt and its effect on hydrocarbon accumulations. In proceedings of the EGPC 9th exploration and production conference, Cairo. EGPC Bulletin 2, 1–19.

Taha, M.A., (1992). Mesozoic rift basins in Egypt: their southern extension and impact on future exploration. Proceedings of the 11th Petroleum Exploration and Production Conference, Cairo, 1988. EGPC, 1–19.

Tissot, B.P., Welte, D.H., (2013). Petroleum formation and occurrence. Springer Science and Business Media.

Van Krevelen, D.W., (1982). Development of coal research—a review. Fuel 61, 786–790.

Walters, C., (2006). The origin of petroleum In: Practical Advances in Petroleum Processing, New York, NY: Springer New York, pp. 79-101.

Waples, D.W., (1985). Geochemistry in petroleum exploration. IHRDC, Boston, 226.

Wu, W., Grana, D., (2017). Integrated petrophysics and rock physics modeling for well log interpretation of elastic, electrical, and petrophysical properties. Appl. Geophys., 146, 54-66.

Yousef, M., Moustafa, A. R., & Bosworth, W. (2023). Structural and tectonostratigraphic evolution of Matruh Basin, northern Western Desert, Egypt: An example of an inverted rift basin. J. Afr. Earth Sci., 203, 104958.

Zhu, H., Ju, Y., Huang, C., Han, K., Qi, Y., Shi, M., Yu, K., Feng, H., Li, W., Ju, L., Qian, J., (2019). Pore structure variations across structural deformation of Silurian Longmaxi shale: an example from the chuandong thrust-fold belt. Fuel 241, 914–932.

Zou, C., Mao, L., Tan, Z., Zhou, L., Liu, L., (2021). Geochemistry of major and trace elements in sediments from the Lubei Plain, China: Constraints for paleoclimate, paleosalinity, and paleoredox environment. J. Asian Earth Sci. X, 6, 100071.